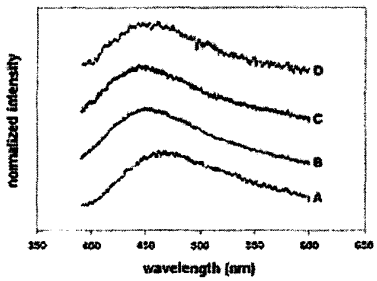

CThW3 Fig. 1. Fluorescence emission spectra and peak wavelengths for A) free NADH, 469 nm; B) immortalized (normal) cells, 455 nm; C) carcinogen transformed cells, 450 nm; and D) chemoprevented cells, 455 nm.

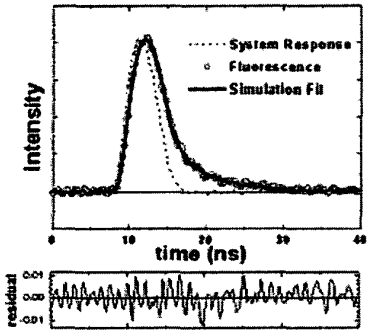

CThW3 Fig. 2. Representative lifetime fit (average lifetime = 2.42 ns) for chemoprevented HBE cells.

2.5 ± 0.1 ns, respectively, which were longer than that of free NADH (0.36 ns).[3,4] Because lifetimes are sensitive to local physical conditions, similar lifetimes among cell lines suggest that the decreased fluorescence intensity observed was due mainly to decreased NADH concentration among cell lines and not due to differing non-radiative decay mechanisms. The increased lifetime of cellular vs. free NADH, as well as the lifetime values reported here, were consistent with those previously reported for protein-bound mitochondrial NADH.[4]

This work illustrates a non-invasive optical method to monitor cellular NADH and probe metabolic activity. Because the HBE cells model various cancer stages, methods used here provide an understanding of the cellular contribution to tissue autofluorescence, leading possibly to optically-based methods for detecting and monitoring cancer progression and treatment.

1. J. Pitts, R. Sloboda, K. Dragnev, E. Dmitrovsky, M.-A. Mycek, "Autofluorescence characteristics of immortalized and carcinogen-transformed human bronchial epithelial cells." *Journal of Biomedical Optics* 6, 31–40 (2001).
2. J. Langenfeld, F. Lonardo, H. Kiyokawa, T. Passalaris, M. Ahn, A. Rusch, E. Dmitrovsky, "Inhibited transformation of immortalized human bronchial epithelial cells by retinoic acid is linked to cyclin E down-regulation." *Oncogene* 13, 1983–1999 (1996).
3. J.D. Pitts, M.-A. Mycek, "Design and development of a rapid acquisition laser-based fluorometer with simultaneous spectral and temporal resolution." *Review of Scientific Instruments* 72, 3061–3072 (2001).
4. M. Wakita, G. Nishimura, M. Tamura, "Some characteristics of the fluorescence lifetime of reduced pyridine nucleotides in isolated mitochondria, isolated hepatocytes, and perfused rat liver in situ." *Journal of Biochemistry* 118, 1151–1160 (1995).
5. A.J. Papadopoulos, N.N. Zhadin, M.L. Steinberg, R.R. Alfano, "Fluorescence spectroscopy of normal, SV40-transformed human keratinocytes, and carcinoma cells." *Cancer Biochemistry Biophysics* 17, 13–23 (1999).

CThW4 **6:00 pm**

Biophotonic Crystal Effects in Multi-modal Nonlinear Microscopy

Shi-Wei Chu, I-Hsiu Chen, Tze-Min Liu, and Chi-Kuang Sun, Graduate Institute of Electro-Optical Engineering, National Taiwan University, Taipei, 10617 Taiwan, R.O.C., Email: r8941009@ee.ntu.edu.tw.

Ping Chin Cheng, Department of Electrical Engineering, State University of New York, Buffalo, NY 14260-2050, USA

Bai-Ling Lin, Molecular and Cell Biology Division, Development Center for Biotechnology, Taipei 10659 Taiwan, R.O.C.

Sue-Ping Lee, Institute of Molecular Biology, Academia Sinica, Taipei 11529, Taiwan, R.O.C.

Photonic crystals are materials with a dielectric property periodicity, which results in linear or nonlinear light property modulation.[1] Recent studies on man-made nano-periodic structures indicate strong enhancement in second-harmonic-generation (SHG)[2] due to the break down of optical centro-symmetry within the materials. Such SHG enhancement by the existence of photonic crystal effect has also been demonstrated using Hyper-Rayleigh scattering recently.[3] Therefore, it is reasonable to speculate that the highly organized biological nano-structures may all behave as nonlinear photonic crystals. Examples of highly organized biological nano-structures include stacked membranes, such as myelin sheath, endoplastic reticulum, grana in the chloroplast, Golgi apparatus, microfibrils and collagen bundles. Here we present a study using a multi-modal nonlinear microscopy,[4] which reveals nonlinear optical activities in those naturally occurring biophotonic crystalline structures. This technique, based on a femtosecond Cr:forsterite laser at 1230 nm, combines different imaging modalities including second-, third-harmonic generations, and multi-photon fluorescence.

Plant cell wall consists of microfibrils orderly arranged to form macrofibrils. This crystalline structure provides active SHG. Figure 1A shows the micro-spectrum measured from the cell wall in maize stem. THG and SHG centered at 410 and 615 nm can be observed. Strong THG is induced by optical inhomogeneity. The biophotonic crystal effect on SHG generation is further confirmed by the significant SHG from the stone cell of pear fruit (Figure 1B) with extensive secondary wall development of the sclerenchyma. Moreover, starch granule consists of crystalline amylopectin lamellae organized into effectively spherical blocklets and large concentric growth rings. These structural features are responsible for the strong SHG that we observed (Figure 1C). Its alternating crystalline and semi-crystalline rings with spatial modulated nonlinear properties could behave as 3D nonlinear photonic "bandgap" crystals[1] and provide possible phase matching mechanism.

The SHG intensity can vary according to the orientation of bio-photonic structures. For instance, by varying the incident light polarization (shown as arrows in Figure 2B-2D), the concentric silica deposition in the dumb-bell-shaped silica cells of rice leaf produces orientated SHG images in respecting to the orientation of the illumination polarization. In contrast, no polarization dependency was found in THG images (Figure 2A). This mechanism provides opportunity for structural studies using SHG with controlled illumination polarization. Apart from mineral deposition in plant cells, laminated membrane structures are also potential candidates for producing strong SHG activity. In chloroplasts, in addition to the 2PF signals (Figure 2H) generated from the auto-fluorescing photosynthetic pigments, THG and SHG appear

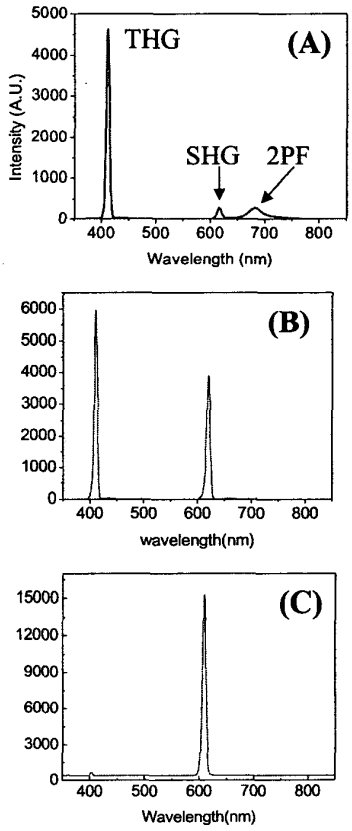

CThW4 Fig. 1. Emission spectra from various biophotonic crystalline structures excited by a 1230 nm femtosecond Cr:forsterite laser. (A) is from the cell wall of maize (*Zea mays*) stem, (B) pear (*Pyrus serotina* R.) stone cell, and (C) potato (*Solanum tuberosum* L.) starch granule. Same excitation intensity and signal integration time were applied.

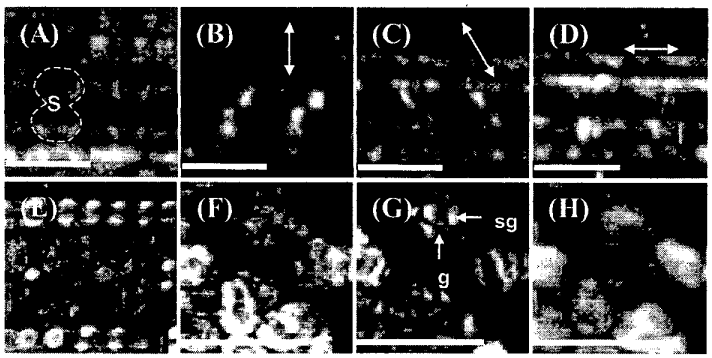

CThW4 Fig. 2. (A) is the THG image showing dumb-bell-shaped silica cells whereas (B)–(D) show the orientation of SHG images change with laser polarization (shown as arrow). (E) is the paradermal TEM image showing silica cells. (F)–(H) are scanning images corresponding to THG, SHG, and 2PF from chloroplasts inside a live mesophyll cell from *Commelina communis* L. showing sub-organellar structures. Scale bar: 15 μm. s: silica cell. g: grana. sg: starch granule.

in different sub-organelle compartments (Figure 2F, 2G). Matching with TEM images, we concluded that the SHG signals are the result of the orderly stacked thylakoid membranes in grana and the highly birefringent starch granules inside the chloroplasts. The stacked thylakoid membranes of grana and the orderly deposited amylopectin in the starch granules provide the structural requirement for efficient SHG resembling the behavior of photonic crystals. Our results reveal photonic crystal-like optical activity in living cells using a multimodality microscopy. This type of highly-penetrative yet noninvasive microscopy is useful for investigating the dynamics of structure-function relationship at the molecular and subcellular levels.

References

1. V. Berger "Nonlinear photonic crystals," *Phys. Rev. Lett.* **81,** 4136 (1998).
2. T.Z. hao *et al.* "Enhancement of second-harmonic generation in BaTiO3/SrTiO3 superlattices," *Phys. Rev. B* **60,** 1697 (1999).
3. K. Clays, S.V. Elshocht, M. Chi, E. Lepoudre, and A. Persoons "Bacteriorhodopsin: a natural, efficient (nonlinear) photonic crystal," J. Opt. Soc. Am. B **18,** 1474 (2001).
4. S.W. Chu, I.S. Chen, T.M. Liu, B.L. Lin, P.C. Cheng, and C.K. Sun "Multimodal nonlinear spectral microscopy based on a femtosecond Cr:forsterite laser," to be published in Optics Letters.

CThW5 **6:15 pm**

Efficient Singlet Oxygen Photosensitization Upon Two-photon Excitation of Porphyrins

Aliaksandr Karotki, Mikhail Drobizhev, Aleksander Rebane, Department of Physics, Montana State University, Bozeman, MT 59717 USA, Email: rebane@physics.montana.edu

Mikalai Kruk, Institute of Molecular and Atomic Physics, National Academy of Sciences, 220072 Minsk, Belarus, Email: kruk@imaph.bas-net.by

Eric Nickel, Synar Technologies, Inc., 1267 Briarwood Drive, Atlanta, GA 30306, USA

Charles W. Spangler, Department of Chemistry and Biochemistry, Montana State University, Bozeman, MT 59717, USA

Use of porphyrin photosensitizers in photodynamic therapy (PDT) is gaining acceptance worldwide as an alternative treatment of tumors[1] and age-related macular degeneration.[2] Utility of porphyrins is based on their special ability to accumulate in pathologic cells, and to transfer absorbed photon energy efficiently to extremely active singlet oxygen molecules, which then wipe out the surrounding tumor. So far, the limited penetration depth by visible light into biological tissue has allowed only few types of skin, breast and certain endoscopically accessible cancers to be treated in this fashion. It has been proposed that by utilizing two-photon absorption (TPA), in which case illumination is carried out at near-IR wavelengths, the PDT may be delivered deeper into the tissue. However, tetrapyrrolic photosensitizers studied so far display disappointingly small TPA cross-sections, typically on the order of $_T\sigma_{PA}$ = 1 – 10 GM (1 GM = 1 · 10^{-50} cm^4 · s/photon).[3]

Here we introduce new porphyrin photosensitizers with greatly enhanced TPA cross-section in near-IR range of wavelengths. One particular example is 5-(4-diphenylaminostilbene), 15-(2,6-dichlorophenyl)-21H,23H-porphine hereafter referred as DPASP. The design of DPASP was based on structure-property relationships, empirically known to enhance TPA cross-section in organic π-conjugated chromophores.[4,5] In this case introduction of a 4-(diphenylaminostilbene)-substituent into the meso-position of the tetrapyrrol ring results in 20 times enhancement

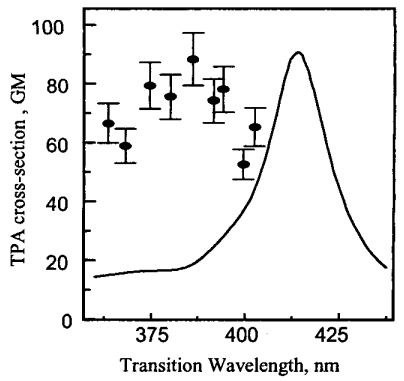

CThW5 Fig. 1. One- (solid) and two- (dash) photon absorption spectra of DPASP in toluene.

in TPA cross-section at λ_{exc} = 780 nm. We demonstrate for the first time that efficient two-photon-excited singlet oxygen generation is achieved by using an allowed transition between the states with the same parity, i.e. the *g-g* transition.

Ti:sapphire regenerative amplifier (CPA-1000, Clark MRX) was used to pump an optical parametric amplifier, OPA, (TOPAS, Quantronix), which yielded 100-fs laser pulses in the wavelength range from 1.1 to 1.6 μm. TPA spectra were obtained by tuning the OPA with second harmonic crystal at the output and registration of one-photon fluorescence.

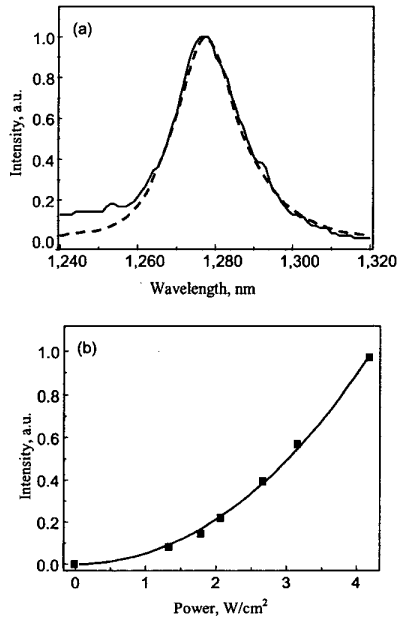

CThW5 Fig. 2. (a) The $^1\Delta_g \rightarrow {}^3\Sigma^-_g$ luminescence spectra of molecular oxygen in toluene. Dashed and solid curves represent, respectively, the spectra measured with one- and two- photon excitation. Both spectra are normalized to unity. (b) The dependence of the oxygen luminescence intensity *I* on the average laser intensity *P* upon two-photon excitation. Experimental data are shown by black squares. Solid curve is the best power-law fit $I = P^n$ with $n = 2.1 \pm 0.1$.